J. Fluid Mech. (1990), *vol.* 215, *pp.* 309–329
Printed in Great Britain

A numerical bifurcation study of natural convection in a tilted two-dimensional porous cavity

By D. S. RILEY[1] AND K. H. WINTERS[2]

[1]School of Mathematics, University of Bristol, Bristol BS8 1TW, UK

[2]Theoretical Physics Division, Harwell Laboratory, Didcot, Oxon OX11 0RA, UK

(Received 2 May 1989 and in revised form 3 November 1989)

Techniques derived from bifurcation theory are used to study the porous-medium analogue of the classical Rayleigh–Bénard problem, Lapwood convection in a two-dimensional saturated porous cavity heated from below. The objective of the study is the explanation of how the multiplicity of solutions observed for lower boundary heating evolves to an apparently unique solution for sidewall heating. The change in boundary conditions from floor to sidewall heating can be effected by smoothly tilting the cavity through 90°. The present study aims to demonstrate the mechanisms that reduce the multiplicity for increasing tilt angle.

The many solutions in the untilted cavity arise from a complex bifurcation structure. The effect of tilting the cavity is to unfold all bifurcations, except those that break the centro-symmetry, and so to create branches disconnected from the primary flow. As the angle of tilt, ϕ, increases most of the limit points at which these branches arise move to higher Rayleigh number Ra. Unexpectedly, for a square cavity, the critical Rayleigh number of the most important limit point (that gives rise to an anomalous stable unicellular flow) is found to be almost independent of the angle of tilt. Moreover the two branches arising at this limit point merge again at higher Rayleigh number to form a continuous closed loop, or isola. As the tilt increases, the upper limit point approaches the lower one until they coalesce at an isola formation point at a critical angle ϕ_c of 10.72°, the maximum angle at which this anomalous mode can exist. Symmetry-breaking bifurcations destabilize part of the branch and determine a smaller critical angle of 10.23°, the maximum angle for which the anomalous mode is stable. At very small angles of tilt, the path of limit points forms the expected cusp catastrophe in the (ϕ, Ra)-plane and at larger angles the path itself turns back at the isola formation point.

The results reveal as too simplistic the conjecture that the reduction of multiplicity for increasing tilt derives from the movement of disconnected branches to increasingly higher Rayleigh number. The predicted collapse and disappearance of branches at an isola formation point is a further novel mechanism which ensures that only the unicellular primary branch remains at a tilt of 90°, in accord with the expected uniqueness of the flow in a square cavity with sidewall heating.

1. Introduction

Convective flows in porous media are of interest in many varied practical situations: in radioactive waste disposal, geothermal energy resource and oil-reservoir modelling, in mass transfer through snow layers and the genesis of

avalanches, in open-pore insulation systems and in gas flows through tobacco rods, to name but a few. These sorts of applications, together with the fact that porous-media flows are of fundamental scientific interest, have motivated a rapidly increasing number of investigations in the last decade. A recent survey of the literature on free-convective flows in porous media may be found in the excellent review by Bories (1985).

The present study is concerned with the bifurcation structure associated with steady free convection in a finite two-dimensional saturated porous cavity heated from below. The aim of the study is to investigate by numerical techniques the unfolding of the bifurcations as the cavity is tilted. An important aspect that we address is the way in which the multiplicity of solutions found for lower boundary heating reduces to leave a unique solution for sidewall heating.

Beck (1972) seems to have been the first to consider convection in a finite three-dimensional horizontal box of porous material saturated with fluid and heated from below. Using linear stability analysis, he found the critical Rayleigh number for the onset of convection in a box of aspect ratios h_1, h_2 (ratio of horizontal dimensions to vertical height). In the present two-dimensional study we are effectively restricting ourselves to thin two-dimensional boxes with length equal to the height ($h_1 = 1$, $h_2 \ll 1$). In most practical situations, the flow would probably be three-dimensional, and indeed the majority of experimental work is concerned with such flow. It is worth stressing, however, that two-dimensional flows do exist both in nature and in the laboratory. Furthermore, the understanding gleaned from two-dimensional studies is essential in facilitating progress in the analysis of the fully three-dimensional situation.

Extensive experimental work on the inclined box has been carried out by Bories and his coworkers: see Bories & Monferran (1972), Bories & Combarnous (1973), Bories, Combarnous & Jaffrennou (1972), Jaffrennou & Bories (1974) and also Hollard (1984). The cell used in this work was of large lateral extension, $h_1 = 9$ and $h_2 = 13$, approximately, where h_2 is the aspect ratio associated with the length along the slope. The results are summarized in figure 1: when the Rayleigh number is small there is a weak unicellular flow whatever the angle of inclination ϕ. When $Ra\cos\phi > 4\pi^2$ and the inclination is between 0° and 15°, polyhedral cells with a vertical axis are observed. For ϕ varying between 15° and ϕ^*, where $Ra\cos\phi^* = 4\pi^2$, longitudinal rolls with axes along the line of greatest slope are superimposed onto the basic unicellular flow, resulting in a helicoidal motion. A single unicellular flow is maintained, even for angles greater than 90°, when $\phi > \phi^*$. An unsteady oscillating flow, characterized by longitudinal rolls oscillating about their axis, is obtained when the layer is inclined and the $Ra\cos\phi$ product is greater than about 250. For larger values of the Rayleigh number there exists fluctuating multicellular flow with continuous creation and disappearance of convective cells, similar to the regime found by Caltagirone, Cloupeau & Combarnous (1971). Kaneko (1972) observed motion consisting of transverse rolls; Jaffrennou & Bories (1974) found similar results and also determined, for a layer of finite extension, the transition conditions between unicellular flow and helicoidal flow. Kaneka, Mohtadi & Aziz (1974), using a cell $18 \times 6 \times 3$ inches high, found that the vigour of the motion, which consisted of transverse rolls, was maximized at a tilt angle of about 10°. For angles greater than about 20°, unicellular flow was approached.

Vlasuk (1972) determined numerically the variation of the global heat transfer with tilt angle, and found that the Nusselt number is maximized at an angle of about 50° for Rayleigh numbers in the range 100 to 350. This was also found by Holst &

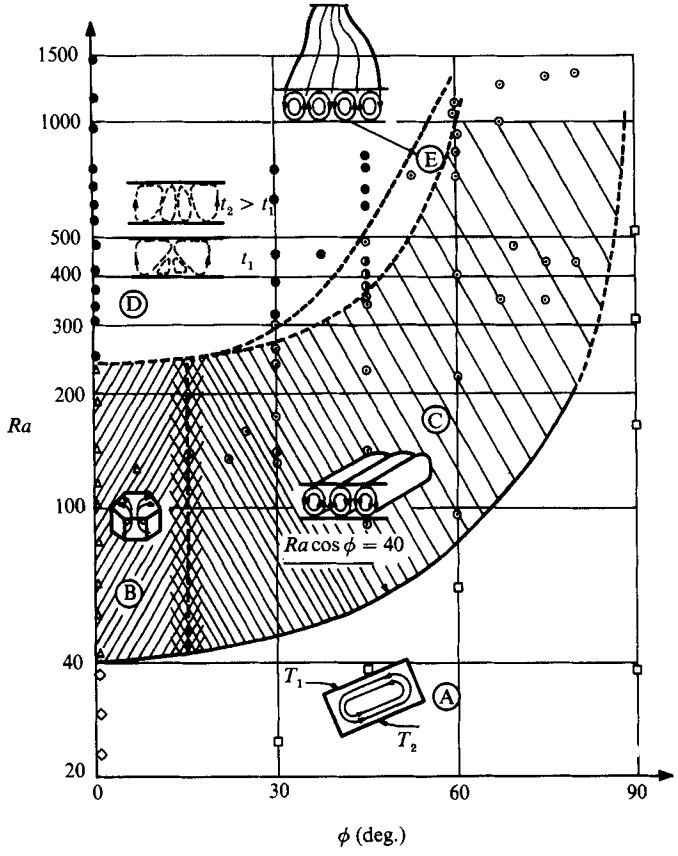

FIGURE 1. The different experimentally determined types of flow in an inclined cell of large lateral extension (after Bories *et al.* 1972). A: unicellular flow; B: polyhedric cells; C: helicoidal cells; D: unsteady regime; E: oscillating helicoidal cells.

Aziz (1972), who investigated a square cavity saturated by a fluid with temperature-dependent properties. Weber (1975) demonstrated that, in a layer of infinite extension, longitudinal rolls constitute the preferred mode of disturbance. Walch & Dulieu (1979, 1982) analysed convection in slightly inclined two-dimensional cavities and showed that anomalous modes exist for inclinations less than 7°. Chan, Ivey & Barry (1970), Walch (1980) and Caltagirone & Bories (1980) studied the existence of, and transitions between, different flow configurations by means of two- and three-dimensional numerical simulations using spectral and finite-difference methods.

Using analytical and numerical (spectral) methods, Caltagirone & Bories (1985) determined two- and three-dimensional solutions for the inclined box and examined their stability. Their results, which are summarized in figure 2, confirmed previously known results for layers of large lateral extent: the existence of three major regimes and the condition for transition from unicellular flow. In addition the study determined: (i) the existence of a transition angle ϕ_t characterizing the change from polyhedric cells to longitudinal coils. The theoretical value was found to be 31° 48′ which differed markedly from the experimental estimates of $\phi_{exp} \sim 15°$; (ii) the critical nature in which initial conditions affected the selection of the mode, when ϕ is less than ϕ_t. It should be emphasized that three-dimensional flows occur naturally

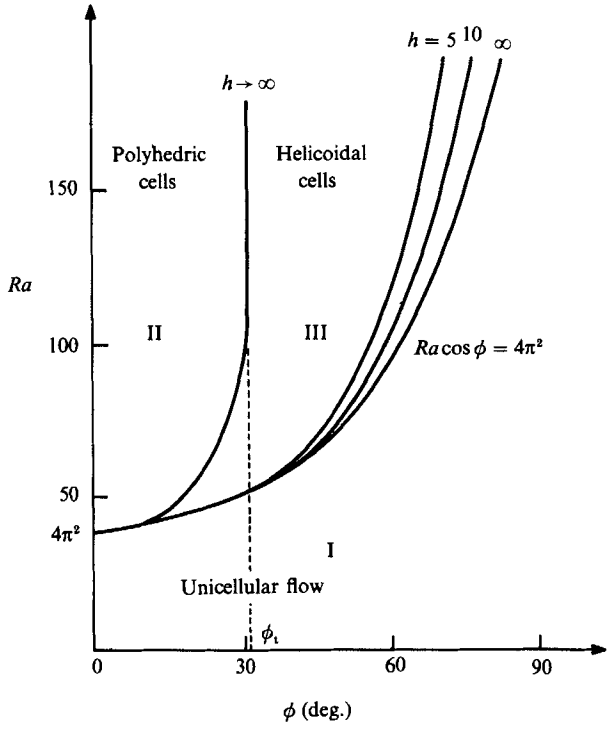

FIGURE 2. The different theoretically determined types of flow in an inclined cell of square cross-section and infinite depth (after Caltagirone & Bories 1985).

in cells of large lateral extent, where such disturbances are easily accommodated. If, however, the third dimension is small the flow may well remain two-dimensional. Thus two-dimensional studies are of real importance.

Recently Riley & Winters (1987, 1989) and Moya, Ramos & Sen (1987) have carried out numerical studies of the two-dimensional problem. In the latter work, the authors found steady solutions to the governing equations using a finite-difference approximation. Their approach was rather limited in that they used a false-transient explicit method to solve the energy equation, and they found only stable solutions. Consequently the bifurcation picture was incomplete and the structure was neither fully determined nor interpreted. Moreover steady solutions proved difficult to obtain using the time-dependent formulation when the parameters lay near stability boundaries (see Sen, Vasseur & Robillard 1987) because the transients in the problem decayed very slowly.

The numerical techniques which we adopt in the present study originate in bifurcation theory. The basic idea is to extend the set of governing equations with conditions that are satisfied at the bifurcation point which is to be located. Partial differential equations can readily be treated by combining this extended-systems approach with the finite-element approximation. The approach has been used with considerable success in a number of related studies, some of which are summarized by Winters, Cliffe & Jackson (1984, 1987). We note that it is natural in the finite-element method to use a direct solver and this makes available the Jacobian matrix $\boldsymbol{f}_x$; this is particularly appropriate for bifurcation studies where the Jacobian can be used for parameter continuation (Keller 1977) and for assessing stability.

The plan of the rest of the paper is as follows: in §2 the governing equations are

formulated. There is then a discussion of the symmetries that the equations possess. In §3 we sketch out the numerical techniques used for locating bifurcation points in the solutions of the equations and for parameter continuation of these solutions. In §4 numerical results are presented for a square cavity, first for the case of zero tilt, and then for non-zero tilt. Finally in §5 the findings are summarized.

2. Formulation

2.1. *Problem description*

The assumptions underlying our model of the porous-medium flow are described in Riley & Winters (1989). We consider a two-dimensional rectangular cavity of height H and aspect ratio $h = W/H$, where W is the lateral dimension (width). The cavity, which is inclined at an angle ϕ with respect to the horizontal (see figure 3), comprises a solid matrix of porosity ϵ, permeability K and heat capacity $(\rho c)_s$, saturated by a fluid with thermal expansion coefficient β, of viscosity ν, heat capacity $(\rho c)_f$ and density ρ. The saturated porous medium is taken to have an effective thermal conductivity k_* and heat capacity $(\rho c)_*$ where

$$(\rho c)_* = \epsilon(\rho c)_f + (1-\epsilon)(\rho c)_s. \tag{2.1}$$

The lateral boundaries of the cavity are adiabatic, while the 'upper' and 'lower' boundaries are at isothermal temperatures $T_0 - \frac{1}{2}\Delta T$, $T_0 + \frac{1}{2}\Delta T$, respectively; ΔT is taken to be positive so that the cavity is heated from below. All boundaries are assumed impermeable.

On invoking the Boussinesq approximation, and assuming that the Prandtl–Darcy number is large, convective flows are governed by the dimensionless equations:

$$\nabla^2\psi = Ra\left\{\frac{\partial\theta}{\partial y}\sin\phi - \frac{1}{h}\frac{\partial\theta}{\partial x}\cos\phi\right\}, \tag{2.2}$$

$$\nabla^2\theta = \frac{1}{h}\left\{\frac{\partial\psi}{\partial y}\frac{\partial\theta}{\partial x} - \frac{\partial\psi}{\partial x}\frac{\partial\theta}{\partial y}\right\} + \frac{\partial\theta}{\partial t}, \tag{2.3}$$

where (x, y) are Cartesian coordinates based at the centre of the cavity,

$$\nabla^2 = \frac{1}{h^2}\frac{\partial^2}{\partial x^2} + \frac{\partial^2}{\partial y^2},$$

t is time, and ψ, θ are stream and temperature functions, respectively. Here Ra denotes the Darcy–Rayleigh number defined by

$$Ra = \frac{g\beta K\Delta T H(\rho c)_f}{\nu k_*}, \tag{2.4}$$

and quantities have been non-dimensionalized using lengthscales H or W (as appropriate), diffusive velocity scale $k_*/H(\rho c)_f$ and the temperature scale ΔT.

The governing equations (2.2), (2.3) hold in the region

$$\Omega = \{(x, y): -0.5 < x < 0.5, -0.5 < y < 0.5\}, \tag{2.5}$$

while on the boundaries we have

$$\psi = 0, \quad \frac{\partial\theta}{\partial x} = 0 \quad \text{on} \quad x = \pm\tfrac{1}{2}, |y| < \tfrac{1}{2}, \tag{2.6}$$

$$\psi = 0, \quad \theta = \mp\tfrac{1}{2} \quad \text{on} \quad y = \pm\tfrac{1}{2}, |x| < \tfrac{1}{2}. \tag{2.7}$$

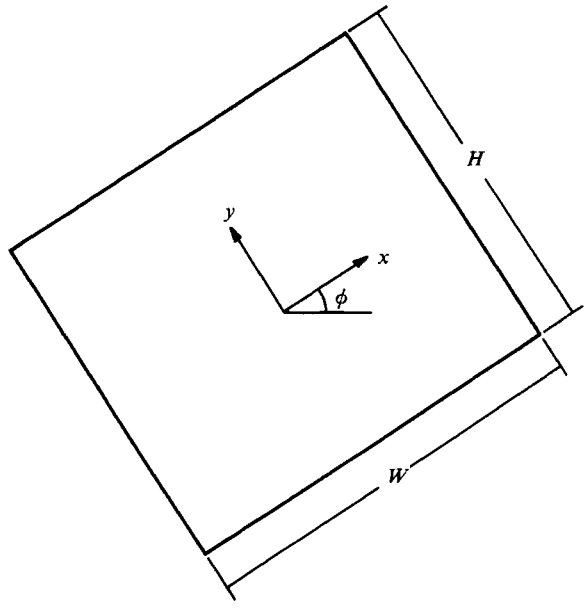

FIGURE 3. The geometry and coordinate system for the two-dimensional rectangular cavity.

2.2. *Symmetries*

When $\phi = 0$ it is straightforward to show that the governing system of equations possesses $\boldsymbol{Z}_2 \times \boldsymbol{Z}_2$ symmetry, where the generators of the group are S_x, S_y defined by

$$S_x\begin{pmatrix}\psi\\ \theta\end{pmatrix} = S_x\begin{pmatrix}\psi(x,y)\\ \theta(x,y)\end{pmatrix} = \begin{pmatrix}-\psi(-x,y)\\ +\theta(-x,y)\end{pmatrix}, \tag{2.8}$$

$$S_y\begin{pmatrix}\psi\\ \theta\end{pmatrix} = S_y\begin{pmatrix}\psi(x,y)\\ \theta(x,y)\end{pmatrix} = \begin{pmatrix}-\psi(x,-y)\\ -\theta(x,-y)\end{pmatrix}. \tag{2.9}$$

The representation Γ of the group $\boldsymbol{Z}_2 \times \boldsymbol{Z}_2$ is $\Gamma = \{I, S_x, S_y, S_x S_y\}$, where I is the identity operator. Here S_x, S_y and $S_x S_y$ represent left–right, up–down, and centro-symmetries respectively.

Again in the untilted case, there exists a solution representing a pure conduction state, viz. $\theta = -y, \psi = 0$. The bifurcations from this trivial solution will have distinct symmetry properties depending on the number of horizontal cells m and vertical cells n. A bifurcation to an odd number of cells in direction i ($i = x$ or y) breaks the symmetry S_i, whilst if $|m-n|$ is odd then the centro-symmetry $S_x S_y$ is broken.

When $\phi \neq 0$ there is no longer a pure conducting solution. The governing system of equations loses the reflection symmetries S_x and S_y but the centro-symmetry $S_x S_y$ is retained. Thus those bifurcations which do not break the centro-symmetry are unfolded under tilt.

It should be noted that the discussion of symmetries by Moya *et al.* (1987) is incomplete. Further, they state that if $\psi(x,y), \theta(x,y)$ are solutions in the untilted case then so are $-\psi(x,y), \theta(-x,y)$; presumably there is a typographical error here and what they are referring to is the symmetry S_x.

3. Numerical methods

The equations (2.2) and (2.3) are discretized in the finite-element approximation using a standard Galerkin formulation with the second-order terms integrated by parts. In the present problem we are mainly concerned with the steady-state solutions of the resulting equations, that is solutions $\boldsymbol{x}$ which satisfy

$$\boldsymbol{f}(\boldsymbol{x}, \lambda, \boldsymbol{\alpha}) = \boldsymbol{0} \tag{3.1}$$

where $\boldsymbol{f}$ is a smooth nonlinear function, λ is a bifurcation parameter, and $\boldsymbol{\alpha}$ is a vector of control parameters. These nonlinear algebraic equations for the unknown values of stream function and temperature are linearized using a Newton–Raphson procedure, and the solution of the linear set of equations at each iteration is obtained using a direct, frontal solver.

The details of how we locate primary bifurcations from the trivial solution; secondary bifurcations (symmetry-breaking or transcritical) from a non-trivial solution; and limit points arising from the unfolding of either primary or secondary bifurcations are all described in Riley & Winters (1989). There we also outline how we use coninuation methods to trace out solution branches, and the loci of bifurcation points as control parameters are varied. In the present problem, isola formation and Hopf bifurcation points also feature.

3.1. *Isola formation points*

Once we have located a limit point we can obtain the variation of the critical bifurcation parameter Ra as one of the control parameters (h, ϕ) varies, to trace out a path of bifurcation points in the two-parameter space (Ra, h) or (Ra, ϕ). This path may itself have a turning point corresponding to an isola formation point. This singular point is located in an identical manner to a transcritical bifurcation.

3.2. *Hopf bifurcation points*

If a generalized eigenvalue of the Jacobian $\boldsymbol{f}_{\boldsymbol{x}}$ becomes purely imaginary, then the equation has a Hopf bifurcation. This gives rise to periodic solutions of angular frequency ω at a critical value of λ, although the Jacobian is not actually singular at that point.

To locate Hopf bifurcations in the steady equations we implement a technique proposed by Jepson (1981) and Griewank & Reddien (1983) in which the following extended set of equations is solved:

$$\begin{pmatrix} \boldsymbol{f}(\boldsymbol{x}_0, \lambda, \boldsymbol{\alpha}) \\ \boldsymbol{f}_{\boldsymbol{x}}(\boldsymbol{x}_0, \lambda, \boldsymbol{\alpha})\,\boldsymbol{\chi}_{\mathrm{R}} + \omega \boldsymbol{M} \boldsymbol{\chi}_{\mathrm{I}} \\ \boldsymbol{f}_{\boldsymbol{x}}(\boldsymbol{x}_0, \lambda, \boldsymbol{\alpha})\,\boldsymbol{\chi}_{\mathrm{I}} - \omega \boldsymbol{M} \boldsymbol{\chi}_{\mathrm{R}} \\ l\boldsymbol{\chi}_{\mathrm{R}} \\ l\boldsymbol{\chi}_{\mathrm{I}} - 1 \end{pmatrix} = \boldsymbol{0}. \tag{3.2}$$

The functions $\boldsymbol{\chi}_{\mathrm{R}}$ and $\boldsymbol{\chi}_{\mathrm{I}}$ are the real and imaginary parts of the right eigenvector of the Jacobian matrix, $\boldsymbol{M}$ is a mass matrix and the last two equations in the set are normalization conditions which use some linear functional l. The solution of these nonlinear equations by Newton's method gives successive approximations to $\boldsymbol{x}_0$, $\boldsymbol{\chi}_{\mathrm{R}}$, $\boldsymbol{\chi}_{\mathrm{I}}$, λ and ω that converge quadratically to their values at the Hopf bifurcation point $\lambda = \lambda_{\mathrm{H}}$, for a good-enough initial guess.

4. Computations

All computations were carried out on a CRAY-1S and CRAY-XMP at Harwell using the finite-element code ENTWIFE. We first used a grid of 8×8 nine-noded elements to determine the state diagram for an untilted cavity. Grid-independence and accuracy checks were then carried out on the locations of the bifurcation points, and continuation methods used to follow these points as the angle of tilt varied. We did not perform exhaustive checks on the accuracy of solutions away from the bifurcation points. For example, in the case of an isola, the limit points were computed to high accuracy, but the solution branches joining these points were not computed to the same accuracy. Our aim in this study is to resolve the effect of tilt on the bifurcation structure, and so the detail of the flow at regular points lies outside our immediate concern. We endeavoured, however, to ensure that we did not introduce spurious bifurcation through using too coarse a grid.

We note that the resolution of the nature of a singular point using either time-dependent finite-difference or modal methods is difficult, especially when other singularities lie nearby. However, the approach of Moya *et al.* (1987) leads to a surprisingly good picture of the possible flows arising from the underlying bifurcation structure. Two remarks concerning their work are perhaps relevant at this point. First, their description seems to suggest that the wider the cavity, the greater the number of points they take in the perpendicular direction; we presume that they actually refine in the parallel direction. Secondly, they remark that the determination of the interface between different cellular regions is difficult and very sensitive to external parameters. Our approach, which allows us to follow unstable solutions and determine bifurcation points exactly, does not suffer from this drawback.

4.1. *Lapwood convection: untilted case*

Before presenting the results on the effect of tilt, we first reproduce the discussion of the results concerning an untilted square cavity from Riley & Winters (1989). The reasons for this are twofold: first to set the new results into a coherent context with consistent labelling of bifurcation points, solution branches and so on. Secondly, to identify the nature of the various branches and to demonstrate clearly the extent of their unfolding.

Figure 4 shows the computed bifurcation structure when $h = 1$ and for Rayleigh numbers up to 350. The measure used in all computed state diagrams is the left-hand mid-wall temperature. In accord with standard practice, the solid and dashed lines indicate stable and unstable branches respectively, and bifurcation points are signalled by solid circles. Primary bifurcations to one-, two- and three-cell modes occur at P_1, P_2 and P_3, respectively. The unicellular mode is stable from onset, while secondary bifurcations $S_{2/1}$ and $S_{3/2}$ stabilize the two- and three-cell modes, respectively. In fact, the three-cell solution branches have two sets of secondary bifurcations at $S_{3/1}$ and $S_{3/2}$. The bifurcation at $S_{3/1}$ is subspace breaking and transcritical, whereas that at $S_{3/2}$, which occurs at a Rayleigh number of 160.25, is centro-symmetry breaking and pitchfork. We note that the crossing at P_3 of the branches arising at the secondary bifurcations $S_{2/1}$ is a consequence of the measure chosen; there are no bifurcations on these secondary branches at this point.

For Rayleigh numbers in excess of 160.25, stable one-, two- and three-cell modes coexist. In theory any of these modes may be observed, but the one-cell mode will be preferred and the multicellular modes will be anomalous under conditions where the Rayleigh number is raised by gradually increasing the applied temperature difference.

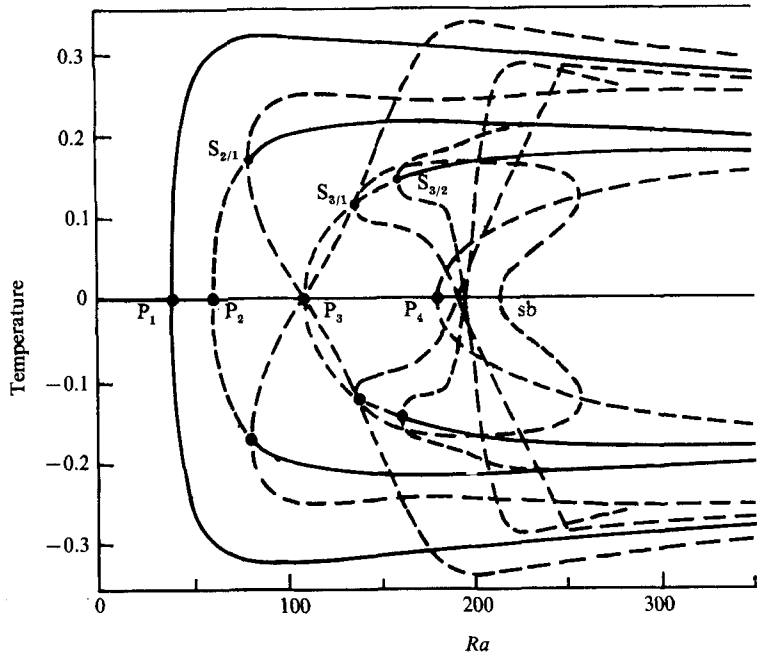

FIGURE 4. Computed bifurcation structure at unit aspect ratio. The measure used is the temperature at $(-0.5, 0)$. Stable/unstable branches are denoted by full/broken curves respectively.

For clarity we have not shown in figure 4 the primary bifurcations located at Rayleigh numbers greater than 180, nor the secondary bifurcations associated with them, nor any tertiary bifurcations (we define a tertiary bifurcation to be a singular point on a branch that arises at a secondary bifurcation). Moreover, a primary bifurcation to a (2, 2) mode occurs at $Ra = 16\pi^2$ but the branch has zero measure (i.e. the left-hand mid-wall temperature remains zero, by symmetry) and overlays the abscissa. A symmetry-breaking secondary bifurcation from this (2, 2) mode occurs at sb and the bifurcating branch connects with the secondary bifurcation at $S_{3/1}$ on the (3, 1) branch. An interesting feature of note is that the primary and secondary branches show a tendency to bunch together at high Rayleigh numbers and they may even meet or cross. This leads to the possible existence of an isola at $\phi = 0$, or to the possibility of isola formation under tilting, with the upper limit point of the isola arising through an unfolding of a transcritical bifurcation formed by the crossing branches. The streamlines and isotherms are displayed in figure 5, where, for clarity, we have not reproduced in full the solution branches. These visualizations graphically confirm the statements concerning symmetry made in §2.2. It should be noted that the flows shown in figures 5(*a*), 5(*e*) and 5(*f*) display the potential to distort into each other when an anticlockwise flow is superimposed; similarly those shown in figures 5(*b*) and 5(*c*) have this same feature.

4.2. *Lapwood convection: tilted case*

In the previous section we described the bifurcation structure as the Rayleigh number varied with both aspect ratio (unity) and tilt (zero) fixed. The effect of varying the aspect ratio of a horizontal cavity is fully discussed in Riley & Winters (1989). In this section we discuss the effect on the bifurcation structure of varying the angle of tilt, with aspect ratio fixed.

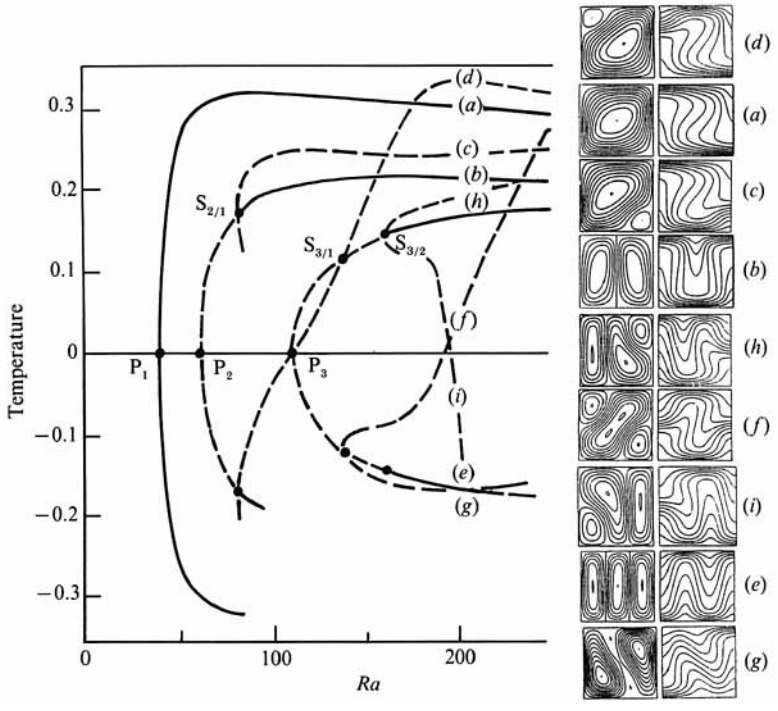

FIGURE 5. Flow visualizations at $Ra = 200$ and $h = 1$. For clarity parts of the solution branches have been omitted. The insets show the streamlines (left) and the isotherms (right). The contour levels are equally spaced between the maximum and minimum values of the stream function and temperature.

We reiterate at this point that, in contrast to aspect-ratio variations which are symmetry preserving, tilting the cavity removes the S_x and S_y symmetries, but preserves the S_xS_y symmetry. Thus any bifurcation which breaks this centro-symmetry will be structurally stable, but other bifurcations will generally be unfolded under tilt. An unfolding of a pitchfork bifurcation (Golubitsky & Schaeffer 1985) is represented schematically in figure 6(*a*), where dashed lines now represent the unfolded solution branches and the open circle demarks a limit point. As the tilt varies the solution norm θ traces a surface shown in figure 6(*b*). The projection of the path of limit points onto the (ϕ, Ra)-plane traces the curve shown, the classical cusp catastrophe. From figure 6(*a*) it is clear that as the Rayleigh number increases at fixed tilt a primary flow develops smoothly along the branch connected to the origin. However, at a critical value of the Rayleigh number two branches disconnected from the primary flow meet at a limit point. Generally one of these is stable and represents an anomalous form of convection. For small enough tilt the anomalous flow will be similar to the primary flow but with an opposite sense of rotation of the convective cells. From figure 6(*b*) we see that this anomalous mode exists at all non-zero values of tilt within the cusp region in the (ϕ, Ra)-plane bounded by the two paths of limit points.

The above description of the unfolding applies to the primary one-cell bifurcation in a square cavity, for tilting the cavity removes the S_x and S_y symmetries that are broken at this bifurcation when $\phi = 0$. Naively one might expect other bifurcations to unfold under tilt in a similar way, resulting in a state diagram with one primary branch connected smoothly to the origin and many disconnected branches arising at

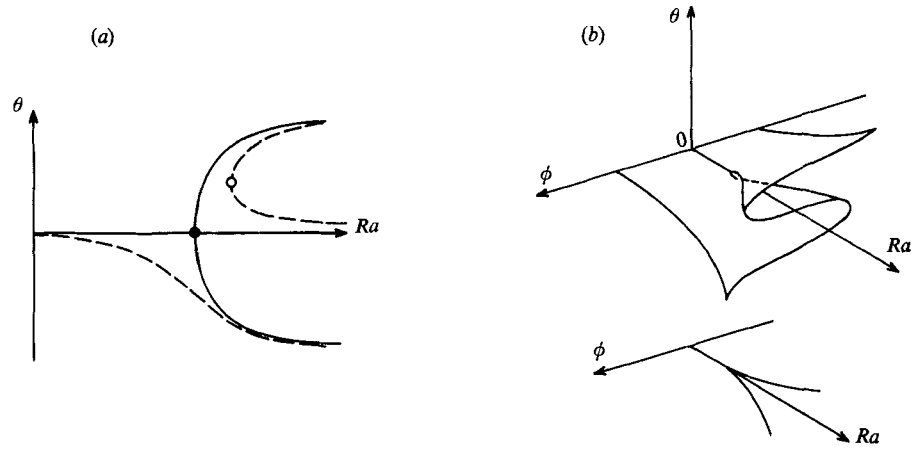

FIGURE 6. Schematic diagram showing effect of tilt. (*a*) The unfolded bifurcation structure at $h = 1$ for small tilt, and (*b*) cusp catastrophe showing the variation of some measure θ of the solution with tilt.

limit points. Then, as the angle of tilt increases, it could be conjectured (cf. Caltagirone & Bories 1985) that the limit points at which the disconnected branches arise move to increasingly larger values of the Rayleigh number, so that at a tilt near to 90° only the primary branch is to be found over a large range of Ra, in accord with the observed uniqueness of the convective flow for conditions of heating from the side. However, two factors modify this view. First, none of the primary bifurcations with $|m-n|$ odd will be unfolded by tilting the cavity, since at these points centro-symmetry is broken for all ϕ. Second, we shall see that a pair of branches arising at a limit point can merge again at a second limit point at higher Rayleigh number to form a continuous closed loop, or isola. With increasing angle of tilt the isola 'shrinks' as the limit points approach one another until at a critical angle of tilt they coalesce and the isola disappears. The critical tilt and Rayleigh number at which this happens defines an isola formation point.

Figure 7 shows the variation with the angle of tilt of the critical Rayleigh number for the appearance of the anomalous unicellular mode in a cavity of unit aspect ratio. This path of limit points, L_1, which was computed on a 32×32 grid, is shown with an enlargement of the small-ϕ region to emphasize the cusp shape anticipated in figure 6. An unexpected feature apparent from figure 7 is that the path of limit points itself has a turning-point (at I_1). Thus for a given value of tilt, not too small, there are two limit points at different Rayleigh numbers and the anomalous branch has the form of an isola of centro-symmetric modes. This closed loop has a lower limit point at L_1 and an upper one at l_1. Another feature is that the critical Rayleigh number of the lower limit point (L_1) remains approximately constant as the tilt increases. Thus the threshold for the appearance of the anomalous unicellular mode is roughly independent of ϕ, in contrast to our naive picture of anomalous modes moving to increasingly higher Rayleigh number for increasing tilt. Also shown in the figure is the variation with angle of tilt of the Rayleigh number at which the primary two-cell flow bifurcates. This path P_2 behaves in a very similar way to the path of limit points L_1 just described: another isola exists, but this time the upper and lower points p_2 and P_2 are symmetry-breaking bifurcation points rather than limit points and the corresponding modes are asymmetric. We shall see that these bifurcation points

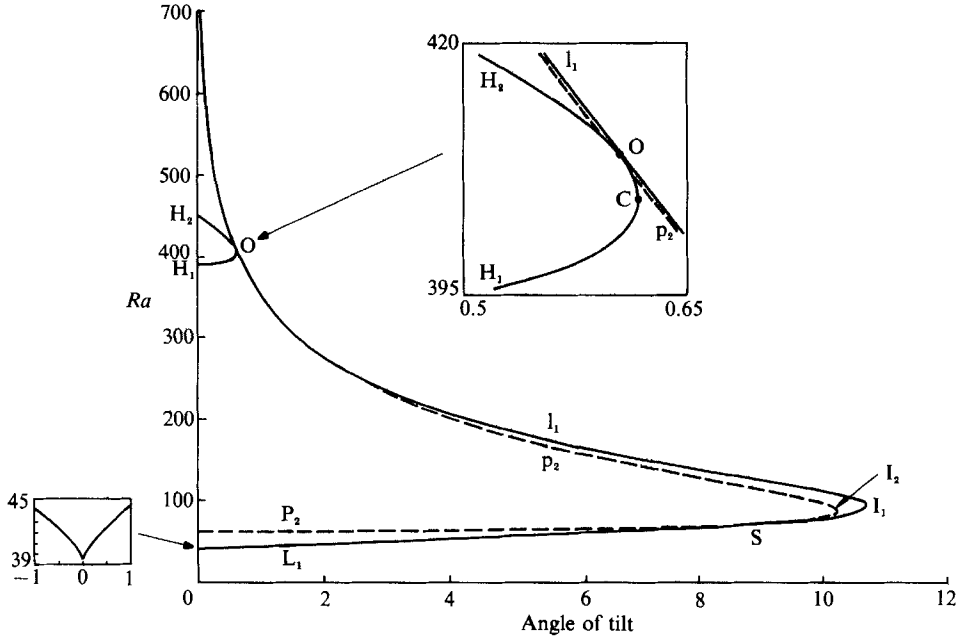

FIGURE 7. Computed variation with tilt of the critical Rayleigh number for the appearance of anomalous primary unicellular flow, represented as the path L_1. The general view shows the paths of limit points L_1 and l_1, pitchfork bifurcation points P_2 and p_2, Hopf points H_1 and H_2, and isola formation points I_1 and I_2. The insets show a close-up of the cusp at small values of tilt, and the osculation of the paths of Hopf points and limit points.

actually lie on the solution branches forming the isola of centro-symmetric modes. Note that there is a double-singular point at S; this corresponds to when the lower bifurcation point passes through the limit point and onto the same solution branch as the upper bifurcation point. This process enables the inner isola to disappear at I_2 through coalescence of the two bifurcation points.

There are several ways to explain the existence/creation of isolas and we have not been able to resolve numerically which of these actually obtains. For example, the isolas may form at a C^- coalesce point, or both the isolas may exist at zero tilt. For this latter case, figure 8 shows schematically a feasible state diagram at zero tilt and its evolution as the tilt angle increases, with particular emphasis on the behaviour at large Rayleigh number. As in figure 5, for clarity we have not shown the full solution structure. Information regarding the eigenvalues of the Jacobian matrix is given along the various solution branches: a plus sign indicates that all the eigenvalues are positive and so the branch is stable. If negative eigenvalues exist then their number is indicated by the number of negative signs on the branch – these branches are unstable. One of the three-cell mixed-mode branches arising at the secondary bifurcation point $S_{3/1}$ on the three-cell branch connects with the one-cell branch at a limit point (l_1) located at a large (possibly infinite) Rayleigh number to form one isola; similarly two-cell mixed-mode branches connect at a pitchfork bifurcation (p_2) from the one-cell branch to form the other isola. Before further discussion of these state diagrams, we need to return to our computed results.

We know from previous studies of the untilted cavity (Kimura, Schubert & Straus 1987; Aidun & Steen 1987) that there is a Hopf bifurcation (denoted by H_1) along the unicellular solution branches at a Rayleigh number of 380. The computed variation

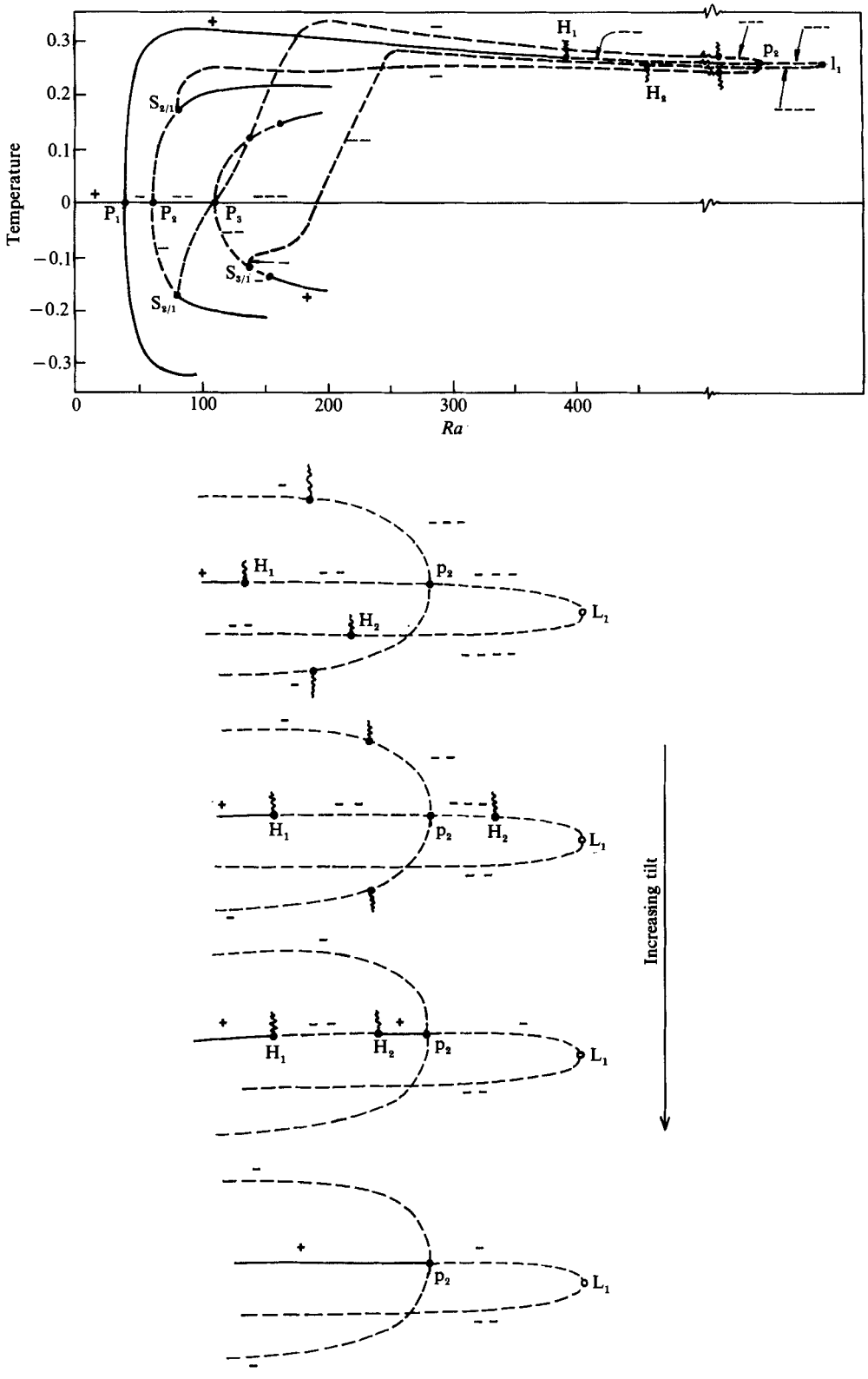

FIGURE 8. Schema showing a possible structure of the state diagram at large Rayleigh number and its evolution with tilt.

with the angle of tilt of the Rayleigh number at which this Hopf bifurcation occurs is shown in figure 7. First, using the extended system (3.2), we located the Hopf bifurcation in the untilted cavity at H_1, which is the Hopf point of lowest critical Rayleigh number. Then by continuation on this point we found that its path turns back at a critical value of ϕ, forming a turning point at C near the path of limit points l_1 associated with the termination of the centro-symmetric isola. The two paths osculate at the point O, and the path of Hopf points returns towards the $\phi = 0$ axis at H_2; flow visualization at zero tilt, see figure 9, reveals that the upper Hopf point H_2 lies on the three-cell mixed-mode branch. On comparing figure 9(*b*) with 5(*f*), we see that the two corner eddies have become very weak, consistent with the notion that the secondary one/three-cell mixed mode mutates into the primary one-cell mode (cf. figure 8). The two Hopf bifurcations interact at C (figure 7) with two possible consequences for the periodic flows arising at these bifurcations: either they are annihilated (at an isola formation point) or disconnected branches of periodic flows are formed (at a coalescence point) – we do not yet have the computational techniques to resolve these different possibilities. We note that the path H_1O marks a transition to oscillatory convection of the anomalous mode.

In figure 8 we show our interpretation of the state diagrams implied by the computed paths of bifurcations. We see that, as the tilt increases, the Hopf bifurcation H_2 moves around the limit point l_1, through the bifurcation point p_2, and then interacts with H_1. It is interesting to note that degree theory implies the existence of further Hopf bifurcations along the asymmetric two-cell mixed-mode branches. As the tilt increases, these unlabelled bifurcations move towards p_2, and coalesce as H_2 passes through p_2.

We now give two specific examples of computed state diagrams at fixed tilt to illustrate the above points concerning isola formation and perfect bifurcation to (2*m*, 1)-mode convection. First, in figure 10(*a*) we show the state diagram, computed on an 8×8 grid, for a cavity of aspect ratio $h = 1$ tilted by 1°. As in the state diagram of figure 4 for the untilted case we plot the temperature at the mid-point of the left wall against Rayleigh number for each of the branches. For reasons of clarity the primary branch which is connected smoothly to the origin has been omitted, and again the limit points arising through the unfolding of pitchfork bifurcation points are denoted by open circles. Also, the branches from $S_{3/2}$ were not computed. The figure clearly shows the features discussed above; the bifurcation to two-cell flow has not been unfolded by tilting and two pairs of branches appear to merge as the Rayleigh number increases. One pair of branches arises at the limit point L_1 on the unfolded one-cell branch and this pair forms the isola discussed in connection with figure 7; from that figure we deduce that the upper limit point l_1 at which the branches merge is at about $Ra = 380$. The other pair of branches arises at the perturbed bifurcation point P_2 and forms a second isola which terminates at p_2 (not labelled), also at about $Ra = 380$. It is interesting that the unfolding creates a mixed composition of primary and secondary modes on the branches shown. For example, considering the first isola which arises at the limit point L_1 on the perturbed one-cell branch, its lower portion connects the perturbed one-cell branch with the perturbed branches of the trivial, primary three-cell, and secondary one/three-cell mixed modes for increasing Rayleigh number. As noted above, the possibility of this continuous evolution of flows is evident from the flow visualizations of figure 5 for the untilted case. Figure 10(*a*) shows that at least five stable solutions exist at high Rayleigh number, in addition to the stable primary flow (not shown). Note that the three-cell branches are stabilized at lower Rayleigh number by the $S_{3/2}$ centro-

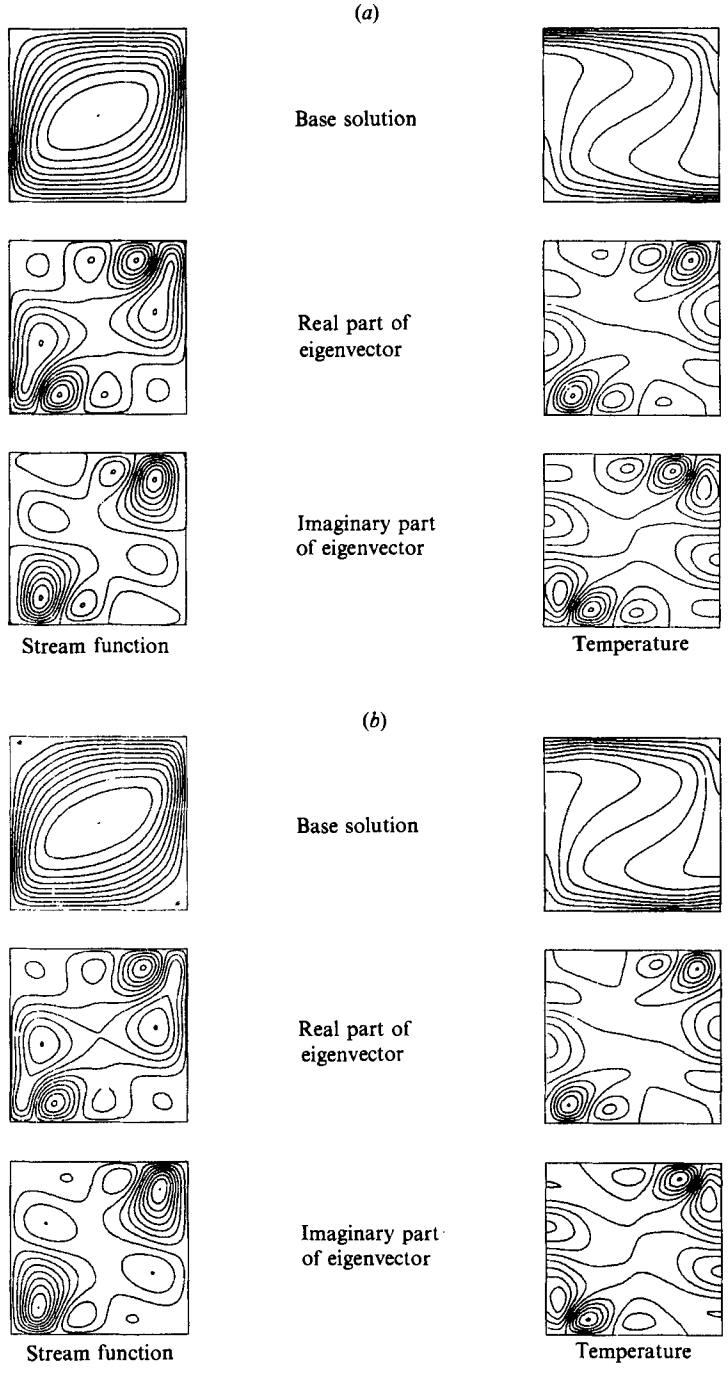

FIGURE 9. Streamlines and isotherms for the steady solution and the real and imaginary parts of the critical eigenvector at the Hopf bifurcation points (*a*) H_1 and (*b*) H_2 when the cavity is untilted.

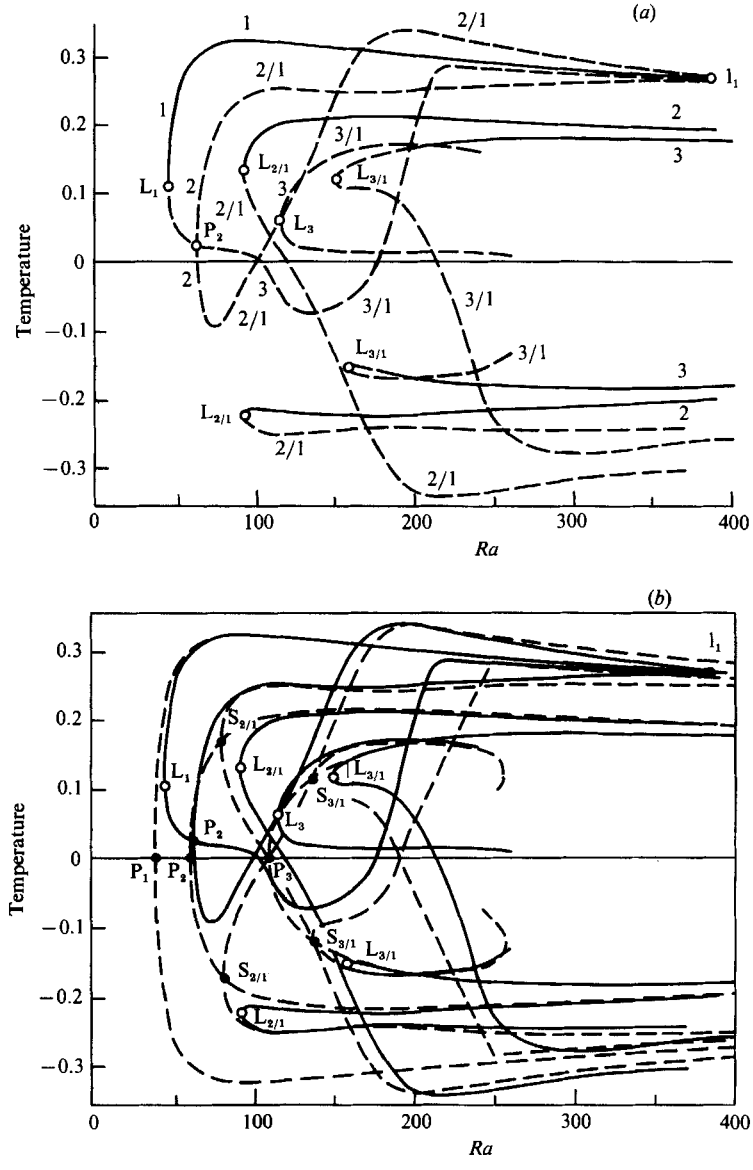

FIGURE 10. (*a*) Unfolding of bifurcation structure at 1° tilt for $h = 1$; the labels indicate the associated branches at zero tilt, and stable/unstable branches are denoted by full/broken curves respectively. (*b*) Composite showing superimposed bifurcation structures at tilts of 0° (broken curves) and 1° (full curves). The measure used is the temperature $(-0.5, 0)$.

symmetry-breaking bifurcations (not shown) which are not unfolded by tilting the cavity. The secondary bifurcation points $S_{2/1}$ and $S_{3/1}$ unfold giving rise to the limit points labelled $L_{2/1}$ and $L_{3/1}$, respectively, while the primary bifurcation point P_3 unfolds and gives rise to the limit point L_3.

To illustrate more clearly the evolution of the solution structure with tilt we present in figure 10(*b*) an overlay of state diagrams for both the untilted and tilted cavities. For the tilted case we have omitted the primary branch connected smoothly to the origin, as in figure 10(*a*). The overlay shows more clearly how the limit points

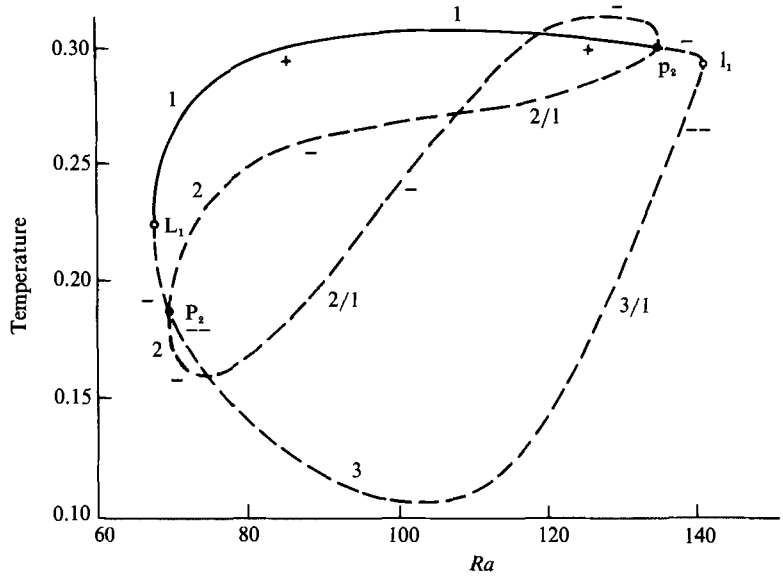

FIGURE 11. Unfolding of bifurcation structure at 7.9° tilt for $h = 1$; the labels indicate the associated branches at zero tilt. A plus sign denotes that all the eigenvalues of the Jacobian matrix are positive. If negative eigenvalues exist then their number is indicated by the number of negative signs on the branch. Stable/unstable branches are denoted by full/broken curves respectively. The measure used is the temperature at $(-0.5, 0)$.

at $\phi = 1$ are generated from the symmetry-breaking bifurcation points at $\phi = 0$ through the unfolding that results from tilting the cavity.

As our second example, in figure 11 we show the computed state diagram for a cavity of aspect ratio $h = 1$ tilted by 7.9°. In this figure all bifurcation points are denoted by solid circles; other crossings are due to the measure we use. The bifurcation of the pair of two-cell branches at P_2 is still apparent and these merge at the bifurcation point p_2 on the centro-symmetric isola; we note that the limit point L_1 on the outer isola is located at $Ra = 67.22$ which is approximately the same value as found for smaller tilt, a feature discussed in connection with figure 7. The stability of the solutions for each of the branches is indicated. In the absence of the symmetry-breaking bifurcation points the one-cell branch would be stable between its upper and lower limit points. The effect of the upper symmetry-breaking bifurcation point is to reduce the range of Rayleigh numbers and tilt angles over which the anomalous solution is stable. Thus the domain over which the anomalous one-cell flow is *stable* is smaller than might be expected from figure 7 and is bounded by $L_1 SI_2 p_2 OH_1$ on that figure.

As the angle of tilt increases from 7.9° we know from figure 7 that the upper and lower limit points, L_1 and l_1, finally coalesce at $\phi = 10.72°$. In order for this to be possible, the second isola shown in figure 11 must first have disappeared through coalescence of the two symmetry-breaking bifurcation points, P_2 and p_2. Clearly one of the symmetry-breaking bifurcation points must first pass on to the same branch as the other for this coalescence to be possible, and so there will be a critical angle at which a symmetry-breaking bifurcation point will coincide with a limit point. This point of coincidence is a codimension-1 singularity known as a double-singular point and is marked S on figure 7.

In the paper by Moya *et al.*, results are included on transitions in tilted cavities

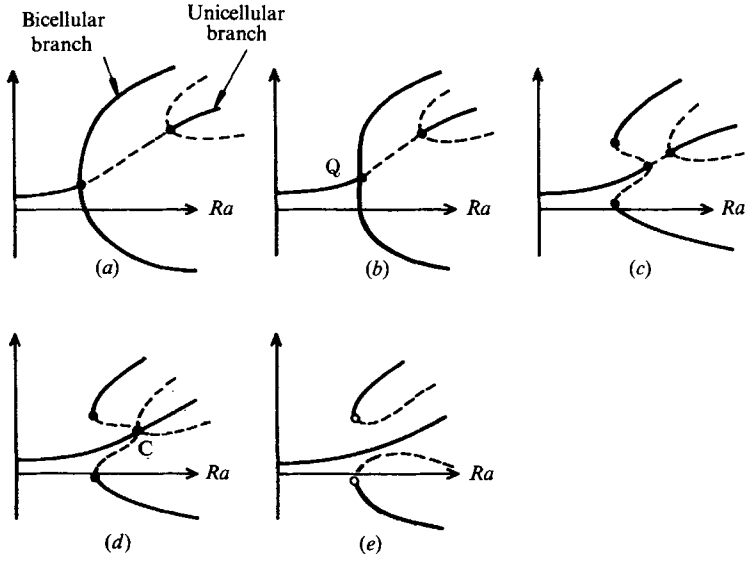

FIGURE 12. Schema showing possible evolution of the state diagram as the tilt increases, leaving the one-cell flow as the unique steady flow. The point Q in (*b*) is a quartic point and C^- in (*d*) is a C^- coalescence point.

between unicellular flows (the baroclinic motion) and flows which are essentially unicellular but which also exhibit secondary cells. We feel that this distinction is not physically significant: the appearance of secondary cells is simply a mutation in the flow pattern and does not arise at a bifurcation. We should stress that the extended-systems approach cannot predict such a phenomenological feature, but it could be identified by monitoring the evolution of the flow along the preferred solution branch. We also note that in their results for a cavity of aspect ratio 10, the bifurcation to multicellular flow appears at Rayleigh number ~ 55 rather than the theoretical value of $4\pi^2$.

So far we have concentrated on a square cavity where a unicellular mode arises at the lowest bifurcation point. As the aspect ratio itself changes we expect that a series of paths similar to that in figure 7 will be traced out. Our experience in analysing the effects of varying the aspect ratio (Riley & Winters 1989) shows that it would be extremely dangerous to presume the bifurcation structure. However, symmetry arguments indicate that anomalous modes must inevitably arise: some at limit points of disconnected branches, others at pitchfork bifurcation points. To illustrate one different structure that might arise, let us consider the situation when the aspect ratio just exceeds $\sqrt{2}$. For this moderate aspect ratio the leading primary mode is bicellular, but we expect that as the tilt increases the unicellular flow will be preferred owing to the smooth evolution of the unicellular branch from the origin. This would then ensure that we recover the expected uniqueness of the flow in a cavity of this aspect ratio with sidewall heating. One possible route to uniqueness, suggested by a related study of Impey, Riley & Winters (1990), is via a coalescence point; the process is shown in figure 12. Note that the secondary bifurcation on the unfolded unicellular branch is pitchfork and the bifurcating solutions break centro-symmetry. The complexity of the route to uniqueness as ϕ tends to 90° increases as the aspect ratio increases, and without extensive computation it would not be a simple matter to determine it.

In our study of the untilted case we demonstrated how secondary bifurcations are necessary for the exchanges of stability to take place as paths of bifurcation points cross with changing aspect ratio. The question which arises naturally is how do these exchanges take place in the tilted case, when at least some of the bifurcations are unfolded? A mechanism for the exchange of stabilities of unfolded bifurcations was proposed by Benjamin (1978) and Schaeffer (1980). The exchange takes place through a complex process which introduces non-degenerate hysteresis and transcritical bifurcation points. The present problem is more complicated in that we have a $Z_2 \times Z_2$ symmetry in which the perturbation (the angle of tilt) unfolds only some of the bifurcations. This process was also considered by Schaeffer (1980) and in future work we shall verify his model through explicit computation.

5. Conclusions

Techniques of bifurcation theory were used previously by Riley & Winters (1989) in a numerical study of Lapwood convection in a horizontal two-dimensional saturated porous cavity. Two particular aspects of the problem were focused upon: (i) the existence of multiple steady solutions and (ii) the influence of aspect ratio. The present work has extended that study to include the effect of tilt on the bifurcation structure for a cavity of fixed aspect ratio.

At an aspect ratio of $h = 1$ we found that all the bifurcations, except those that break centro-symmetry, were unfolded under tilt, giving rise to a primary solution branch associated with a stable unicellular flow and to disconnected branches. As the tilt increased, most of the limit points at which these disconnected branches arise moved to higher Rayleigh number. Unexpectedly, the critical Rayleigh number of the most important limit point, the one which gives rise to an anomalous *stable* one-cell flow, was almost independent of ϕ. Physically this means that the anomalous unicellular flow persists in a tilted cavity, and that alternative stable flows exist at very moderate values of the Rayleigh number. The two branches arising at this limit point merged again at higher Rayleigh number to form an isola, thus determining an upper limit on the Rayleigh number for existence of the anomalous flow at a given angle of tilt. With increasing tilt the upper limit point approached the lower one until they coalesced at a critical angle of tilt $\phi_c = 10.72°$, the maximum angle at which the anomalous one-cell flow can exist. This novel process is thus a further mechanism by which modes disappear to leave a unique unicellular flow in a square cavity with sidewall heating.

A full stability map of the alternative stable unicellular flow is shown in figure 13. This map has been determined by solving the steady equations numerically, and by using the extended-systems approach to compute the boundaries between the flow domains. The determination of such a map by direct numerical solution of the time-dependent equations would, at best, be inefficient, and, at worst, unrealistic. By comparing this with figure 7 we see that, while the domain of *existence* for the anomalous one-cell flow is bounded by the path $L_1 I_1 l_1$, the domain of *stability* of this flow is smaller; it is bounded by $L_1 SI_2 p_2 OH_1$ and is determined by other pitchfork and Hopf bifurcations. The maximum angle at which the anomalous unicellular flow is stable is 10.23° and occurs at I_2. We also show on figure 13 the streamlines and isotherms that describe the anomalous unicellular flow at the isola formation point, the point of maximum tilt I_1 of figure 7. This visualization confirms the anomalous nature of the flow, which rotates in a sense opposite to that expected and flows downward near to the heated slope.

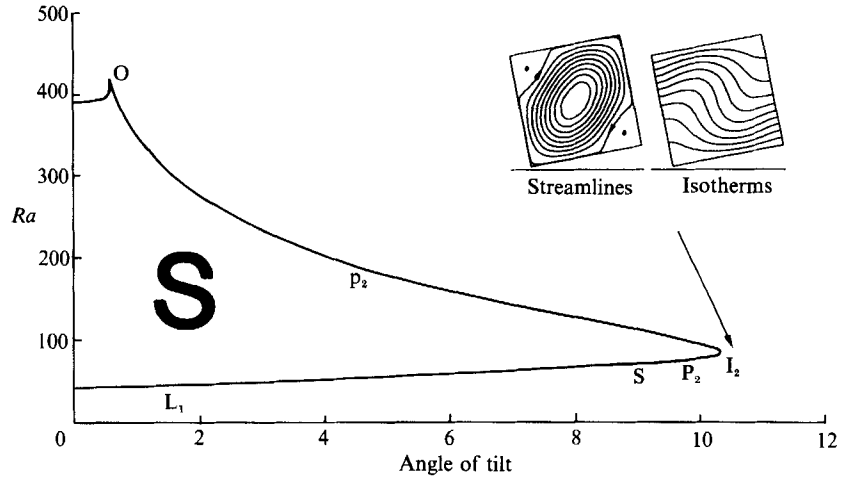

FIGURE 13. Stability map showing the domain over which the anomalous unicellular flow is stable. The path H_1O marks a transition to anomalous oscillatory convection. The streamlines and isotherms at the isola formation point I_1 close to I_2 are also displayed.

Finally we should emphasize that, although we have discussed the effect of tilt in this study, the results apply qualitatively to any imperfection which removes the same symmetries. For example, Impey *et al.* (1990) discuss the effect of sidewall leakage of heat, and uncover analogous processes.

It is a pleasure to thank K. A. Cliffe for many helpful discussions. The work described in this report is part of the longer term research carried out within the Underlying Programme of the United Kingdom Atomic Energy Authority. One of us (D.S.R.) wishes to thank SERC for partial support towards the computing costs of this research programme under Research Grant GR/D/466010.

REFERENCES

AIDUN, C. K. & STEEN, P. H. 1987 Transition to oscillatory convective heat transfer in a fluid-saturated porous medium. *J. Thermophys.* **1**, 268.

BECK, J. L. 1972 Convection in a box of porous material saturated with fluid. *Phys. Fluids* **15**, 1377.

BENJAMIN, T. B. 1978 Bifurcation phenomena in steady flows of a viscous fluid. *Proc. R. Soc. Lond.* A **59**, 1.

BORIES, S. A. 1985 Natural convection in porous media. In *Proc. of NATO ASI on Fundamentals of Transport Phenomena in Porous Media.*

BORIES, S. A. & COMBARNOUS, M. A. 1973 Natural convection in a sloping porous layer. *J. Fluid Mech.* **57**, 63.

BORIES, S. A., COMBARNOUS, M. A. & JAFFRENNOU, J. Y. 1972 Observation des différentes formes d'écoulements convectifs dans une couche poreuse inclinée. *CR Acad. Sci. Paris* A **275**, 857.

BORIES, S. A. & MONFERRAN, L. 1972 Conditions de stabilité et échanges thermiques par convection naturelle dans une couche poreuse inclinée de grande extension. *CR Acad. Sci. Paris* B **274**, 4.

CALTAGIRONE, J. P. & BORIES, S. A. 1980 Solutions numériques bidimensionelles et tridimensionelles de l'écoulement de convection naturelle dans une couche poreuse inclinée. *CR Acad. Sci. Paris* B **190**, 197.

CALTAGIRONE, J. P. & BORIES, S. 1985 Solutions and stability criteria of natural convective flow in an inclined porous layer. *J. Fluid Mech.* **155**, 267.

CALTAGIRONE, J. P., CLOUPEAU, M. & COMBARNOUS, M. A. 1971 Convection naturelle fluctuante dans une couche poreuse horizontale. *CR Acad. Sci. Paris* B**273**, 833.

CHAN, B. K. C., IVEY, C. M. & BARRY, J. M. 1970 Natural convection in enclosed porous media with rectangular boundaries. *Trans. ASME* C: *J. Heat Transfer* **92**, 21.

GOLUBITSKY, M. & SCHAEFFER, D. G. 1985 *Singularities and Groups in Bifurcation Theory. Part I.* Springer.

GRIEWANK, A. & REDDIEN, G. 1983 The calculation of Hopf points by a direct method. *IMA J. Numer. Anal.* **3**, 295.

HOLLARD, S. 1984 Structure thermoconvectives stationnaires dans une couche poreuse plane inclinée de grande extension. Thèse de Docteur-Ingénieur, Institut National Polytechnique de Toulouse.

HOLST, P. H. & AZIZ, K. 1972 A theoretical and experimental study of natural convection in a confined porous medium. *Can. J. Chem. Engng* **50**, 232.

IMPEY, M. D., RILEY, D. S. & WINTERS, K. H. 1990 The effect of sidewall imperfections on pattern formation in Lapwood convection. *Nonlinearity* **3**, 197.

JAFFRENNOU, J. Y. & BORIES, S. A. 1974 Convection naturelle dans une couche poreuse inclinée: influence des effets d'extrémité sur les conditions de stabilité. *Rapport interne* GE14. Institut de Mécanique des Fluides de Toulouse.

JEPSON, A. D. 1981 Numerical Hopf bifurcation. Thesis, Part 2, California Institute of Technology, Pasadena, California, USA.

KANEKO, T. 1972 An experimental investigation of natural convection in porous media. M.Sc. Thesis, University of Calgary.

KANEKO, T., MOHTADI, M. F. & AZIZ, K. 1974 An experimental study of natural convection in inclined porous media. *Intl J. Heat Mass Transfer* **17**, 485.

KELLER, H. B. 1977 Numerical solutions of bifurcation and nonlinear eigenvalue problems. *Applications of Bifurcation Theory* (ed. P. H. Rabinowitz), pp. 359–384. Academic.

KIMURA, S., SCHUBERT, G. & STRAUS, J. M. 1987 Instabilities of steady, periodic, and quasi-periodic modes of convection in porous media. *Trans. ASME* C: *J. Heat Transfer* **109**, 350.

MOYA, S. L., RAMOS, E. & SEN, M. 1987 Numerical study of natural convection in a tilted rectangular porous material. *Intl J. Heat Mass Transfer* **30**, 741.

RILEY, D. S. & WINTERS, K. H. 1987 The onset of convection in a porous medium: a preliminary study. *Harwell Rep.* R 12586.

RILEY, D. S. & WINTERS, K. H. 1989 Modal exchange mechanisms in Lapwood convection. *J. Fluid Mech.* **204**, 325.

SCHAEFFER, D. G. 1980 Qualitative analysis of a model for boundary effects in the Taylor problem. *Proc. Camb. Phil. Soc.* **87**, 307.

SEN, M., VASSEUR, P. & ROBILLARD, L. 1987 Multiple steady states for unicellular natural convection in an inclined porous layer. *Intl J. Heat Mass Transfer* **30**, 2097.

VLASUK, M. P. 1972 Convective heat transfer in a porous layer (in Russian). *4th All Union Heat and Mass Transfer Conf., Minsk.*

WALCH, J. P. 1980 Convection naturelle dans une boîte rectangulaire: contribution a l'étude du cas stable. Thèse, Université Paris VI.

WALCH, J. P. & DULIEU, B. 1979 Convection naturelle dans une boîte rectangulaire légèrement inclinée contenant un milieu poreux. *Intl J. Heat Mass Transfer* **22**, 1607.

WALCH, J. P. & DULIEU, B. 1982 Convection de Rayleigh–Bénard dans une cavité poreuse faiblement inclinée. *J. Phys. Lett. Paris* **43**, L103.

WEBER, J. E. 1975 Thermal convection in a tilted porous layer. *Intl J. Heat Mass Transfer* **18**, 474.

WINTERS, K. H., CLIFFE, K. A. & JACKSON, C. P. 1984 A review of extended systems for finding critical points in coupled problems. In *Conf. on Numerical Methods for Transient and Coupled Problems* (ed. R. W. Lewis, E. Hinton, P. Bettess & B. A. Schrefler), pp. 949–959. Swansea: Pineridge.

WINTERS, K. H., CLIFFE, K. A. & JACKSON, C. P. 1987 The prediction of instabilities using bifurcation theory. In *Numerical Methods for Transient and Coupled Problems* (ed. R. W. Lewis, E. Hinton, P. Bettress and B. A. Schrefler), pp. 179–198. John Wiley.